Nanotechnol. Environ. Eng. (2017) 2:10
https://doi.org/10.1007/s41204-017-0021-z

ORIGINAL PAPER

Potential degradation of hazardous dye Congo red by nano-metallic particles synthesized from the automobile shredder residue

Jiwan Singh[1] · Ajay S. Kalamdhad[2] · Janardhan Reddy Koduru[3]

Received: 9 February 2017 / Accepted: 24 June 2017 / Published online: 3 July 2017

Abstract This study was carried out on the degradation of Congo red (CR) in an aqueous solution by nano-metallic particles (NMPs). The NMPs were synthesized from the leachate of automobile shredder residue. Scanning electron microscopy was performed to analyze the morphology of particles. Fourier transform infrared spectroscopy (FTIR) was also done to demonstrate the possibility and changes of various functional groups before and after the reaction of NMPs. The effect of the dosages of NMPs, pH values of solution, concentrations of CR and H_2O_2 on CR degradation was studied. The results of the present study confirm that the CR degradation rate was improved by increasing the dosages of NMPs and H_2O_2 up to certain limit and then reduced gradually. However, degradation rate was reduced by raising the pH values and concentration of CR. The pseudo-second-order kinetics was found to be suitable for the degradation of CR by NMPs under Fenton-like process.

Keywords NMPs · CR · Kinetics · Mechanism · Degradation

✉ Jiwan Singh
jiwansingh95@gmail.com

✉ Janardhan Reddy Koduru
reddyjchem@gmail.com

[1] Department of Environmental Science, Babasaheb Bhimrao Ambedkar University, Lucknow 226025, India

[2] Department of Civil Engineering, Indian Institute of Technology Guwahati, Guwahati, Assam 781039, India

[3] Department of Environmental Engineering, Kwangwoon University, Seoul 139-701, Republic of Korea

Introduction

The presence of reactive azo dyes in water stream can pose serious environmental problems. These dyes are released from the textile and dyeing industries [1]. Azo dyes have been predicted as potential genotoxic and carcinogenic chemical [2]. Approximately 15% of the dyes are lost during the dyeing process, and then, it released into environment [3]. Congo red (CR) is one of most widely used dye in the textile industries. This dye cannot be efficiently decolorized mainly because of presence of many benzene rings in their structure. Dyes removal from wastewater has been widely studied to reduce its environmental impact. There are different types of techniques available, which are adsorption [4], ozonation [5], Fenton-like degradation [6] and photocatalysis [7]. Fenton-like degradation is a rapid and cost-effective approach, and this is also simple to implant for the industrial scale to remove dyes from the wastewater before discharging into the environment. In the Fenton-like process, hydroxyl radicals are produced by the oxidation using hydrogen peroxide [8]. Currently, nanoparticles have been applied for azo dye removal; these particles are zero-valent iron (Fe^0) [9] and bimetallic nanoparticle, such as Fe/Ni [10]. Adsorptive removal of CR has been studied by some researchers [11–13]. Recently, nano-metallic particles (NMPs) have been considered as a promising agent to treat the organic pollutants from the wastewater [8, 14]. However, application of NMPs for degradation of reactive azo dye (CR) is still limited.

Therefore, the present study was carried on the removal of CR by NMPs in the presence of hydrogen peroxide. NMPs were recovered from the fine fraction of automobile shredder residue (ASR). This has been considered that ASR is highly contaminated with heavy metals [15, 16]. In many countries, ASR waste is dumping into landfills,

which may increase the risk of ground water pollution [15, 17]. The objective of the study was to treat the dye containing wastewater by applying NMPs (recovered from the leachate of ASR).

Materials and methods

The analytical grade chemicals were used in this work. A Congo red ($C_{32}H_{22}N_6Na_2O_6S_2$) sodium borohydride ($NaBH_4$), hydrogen peroxide ($H_2O_2$) and hydrochloric acid (HCl) were supplied by Samchun Pure Chemicals Co. Ltd. (South Korea). Figure 1 shows the molecular structure of Congo red.

The details of the leaching of metals and recovery of NMPs from the ASR have been given in our previous study [14]. The recovery of NMPs was conducted at pH 7 of leachate solution through reduction method by using sodium borohydride ($NaBH_4$). The experiment on CR degradation by NMPs was carried out in conical flasks of 250 mL at 25 °C in a water bath shaker (SWB-35, Hanyang Scientific equipment Co., Ltd., South Korea) at 60 rpm. A 100 mL of CR solution was taken in flasks, and then, suitable amount of NMPs (0.1 g/L, except dose study) and H_2O_2 (50 mM, except H_2O_2 concentration) was added to solution. Experiment was also carried out at different values of pH (pH 2, 3, 4 and 5) of the CR solution, and the pH of CR solution was maintained with 0.1 N HCl and 0.1 N NaOH. A solution of natural pH (6.5) also checked the CR degradation by NMPs. To measure the remaining CR concentration in solution, a 2 mL of sample was taken at various time intervals and then filtered through a 0.25-μm-size filter paper.

To determine the residual concentration of CR, UV–Visible spectrophotometer (UV 1601, Shimadzu) was used at a maximum wavelength (λ_{max}) of 495 nm. The scanning electron microscope (SEM; S–4300CX; Hitachi, Japan) was applied to analyze morphology of NMPs. A Fourier transform infrared (FTIR) spectrophotometer (ISF 66/S, Bruker) was used to describe the functional groups on NMPs before and after reaction. X-ray diffraction (XRD) studies of the NMPs were analyzed using a D/Max–2500 diffractometer (Rigaku, Japan).

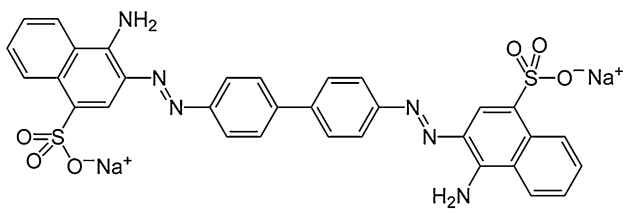

Fig. 1 The molecular structure of hazardous dye Congo red (CR)

The rate of CR degradation by NMPs was determined by a pseudo-first-order reaction model [14],

$$\ln(C_t/C_0) = -k_1 t \quad (1)$$

where C_0 is the initial concentration of CR (mg/L), C_t represents residual concentration of CR at time t (min), and k_1 is the pseudo-first-order rate constant (min^{-1}).

The removal of the CR by NMPs was also studied by a pseudo-second-order reaction kinetics [18],

$$1/C_t = (1/C_0) + k_2 t \quad (2)$$

The slope of the plot between $1/C_t$ and time yields the pseudo-second-order rate constant k_2.

Results and discussion

Characterization of NMPs

Figure 2a represents a SEM image of the prepared NMPs. The results of the SEM analysis revealed that NMPs are not in spherical shape. Most of nanoparticles display a small clumping; this may be due to magnetic interaction by Fe present in NMPs [19]. The diameter of the NMPs was observed ≤100 nm. These NMPs tended to aggregate together to form chain structures, which might be due to the magnetic interaction between small particles [20]. As shown in Table 1, Fe was the most dominated element (54.65%) followed by carbon (26.47%), Zn (11.72%), and Al and Cu (3.02%). However, Ni, Pb and Mn were found to be in trace quantity.

FTIR spectra of NMPs before and after reaction with CR are shown in Fig. 2b. The peak was observed at 1396.7 cm^{-1}; this peak specifies the presence of metals oxides (M–O) bands on the surface of NMPs. However, after reaction this peak was found to be slightly smaller and also shifted at 1413.6 cm^{-1}. M–O band could indicate the M_2O_3 and M_3O_4 which designated partial oxidation of NMPs [14, 21]. The FTIR spectra of NMPs exhibited broaden bands at 3298 cm^{-1}, which describe the O–H stretching [14]. After reaction, this peak was widen and shifted to 3206.5 cm^{-1}. The peak at 1647.9 cm^{-1} represents the O–H stretching; however, intensity of this peak was improved and shifted to 1619.02 cm^{-1} [22]. However, the bands at 1036.3 cm^{-1} were observed after Fenton-like oxidation of CR, conforming the Fe–O stretching about Fe_2O_3 [21]. The XRD results exposed in Fig. 2c characterize the diffraction patterns of the NMPs. The diffraction peaks at $2\theta = 30.8°$ indicate the formation of metals oxides (M_xO_y), where M_xO_y may suggest FeO, Fe_2O_3, Cu_2O, etc. [23, 24]. The NMPs were observed in crystalline metal oxide phase. The broad metal oxide peak implies that the synthesized NMPs hold a chemically disordered crystal

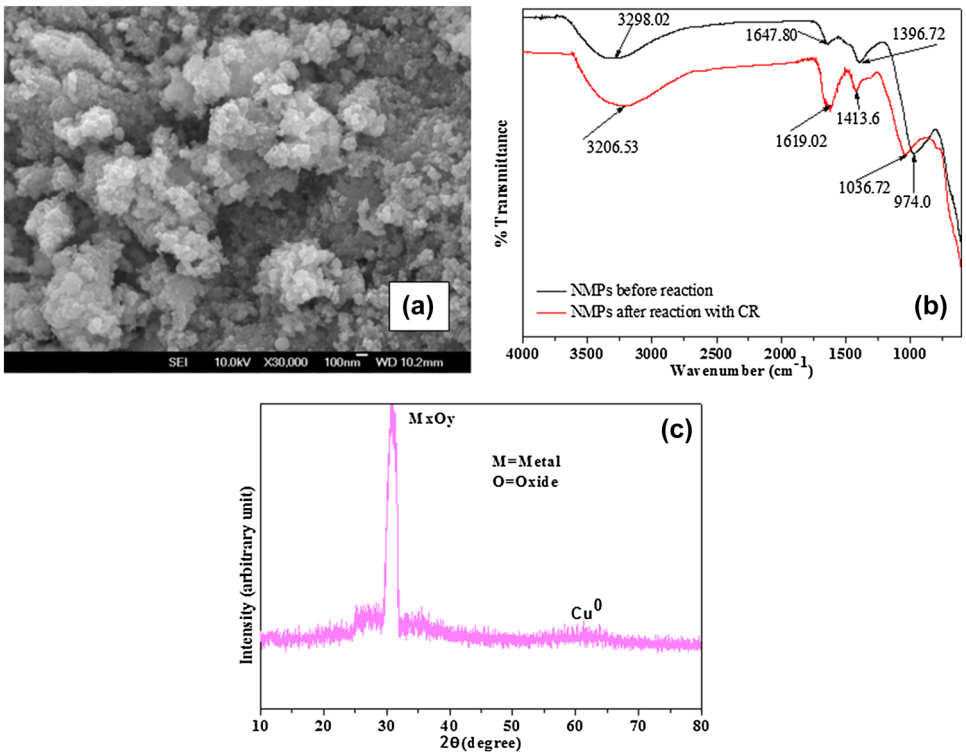

Fig. 2 SEM image of NMPs (**a**) and FTIR analysis of NMPs before and after reaction (**b**)

Table 1 Energy-dispersive X-ray spectroscopy (EDX) analysis of NMPs

Element	Weight (%)
C K	26.27
Al K	3.02
Mn K	0.64
Fe K	54.65
Ni K	0.24
Cu L	3.02
Zn L	11.72
Pb M	0.60
Totals	100.00

structure [25]. The diffraction peaks at $2\theta = 61.2°$ indicate the formation of zero-valent Cu [26].

Degradation of CR by NMPs

Effect of NMPs dosages on CR degradation

The effect of various NMPs dosages (0.025, 0.05, 0.10 and 0.15 g/L) on the reaction rate was carried out at pH—3.0, CR initial concentration—10 mg/L, temperature—25 °C and concentration of H_2O_2—50 mM (Fig. 3a). The degradation efficiency of CR was increased with increasing dosages of NMPs up to 0.10 g/L, and this happened due to the increasing reaction sites [8]. However, with a further increase in dosages of NMPs, degradation efficiency of CR was reduced gradually. This reduction in the degradation efficiency of CR can be attributed to clustering of NMPs during the reaction [27]. Around 95.8% of CR degradation efficiency was attained in the 180 min of reaction time with dose of NMPs of 0.10 g/L. However, removal efficiency of CR was decreased to 91.9% with a dose of 0.15 g/L of NMPs. A high removal of CR by NMPs might be due to the small size of NMPs resulting high surface area. The CR degradation was increased with the increase in the dose of NMPs; this can be due to more availability of reactive site for electron transfer from the surface NMPs to H_2O_2 [28]. The optimum dosage of NMPs was selected as 0.10 g/L for subsequent CR degradation. Figure 4a shows the plot of ln C_t/C_o versus t for the degradation of CR with the different dosages of NMPs. Table 2 shows the values of the pseudo-first-order rate constant (k_1), pseudo-second-order rate constant (k_2) and R^2 for the degradation of CR with different dosages of NMPs. The value of k_1 was increased 21.4% with increasing dose up to 0.10 g/L. A value of k_1 was decreased with increasing dose of NMPs; a similar trend was also followed by k_2 value.

Effect of pH values on CR degradation

A pH can affect the degradation of organic pollutants by NMPs. Acidic nature of dye solution generating more reactive sites on the surface of NMPs, triggering degradation of organic pollutants. However, an extremely acidic pH of solution (pH < 2) initiates fast corrosion of NMPs,

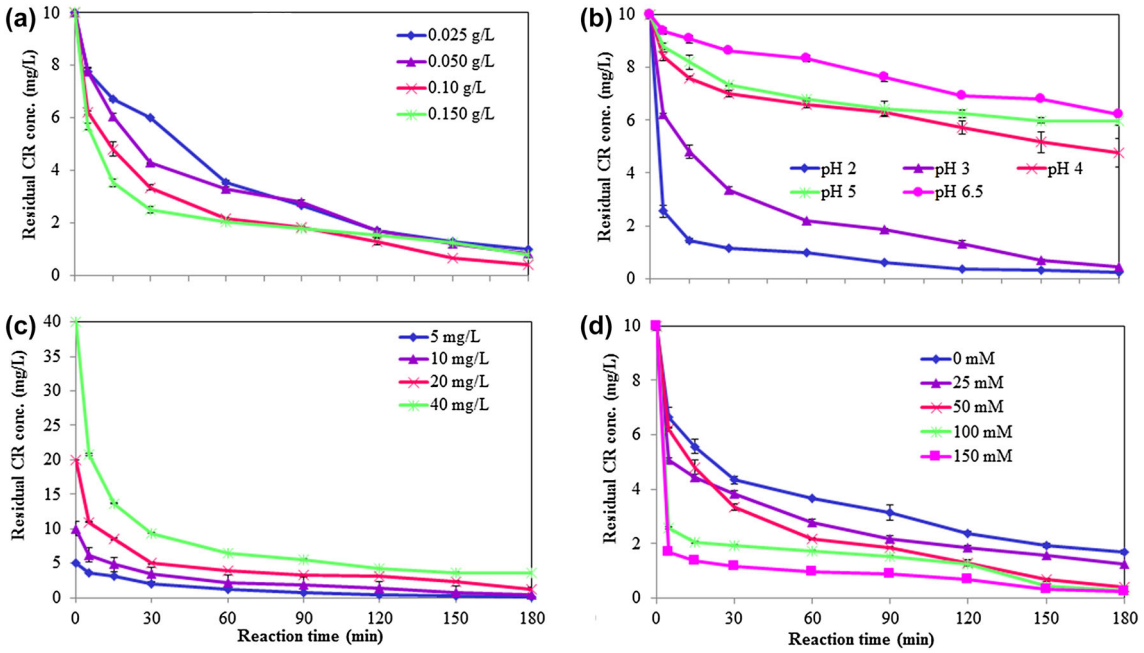

Fig. 3 Effect of the different parameters: effect of dosages of NMPs (**a**), effects of pH values (**b**), effect of initial concentration of CR (**c**) and effect of concentration of H_2O_2 (**d**) on the CR degradation process

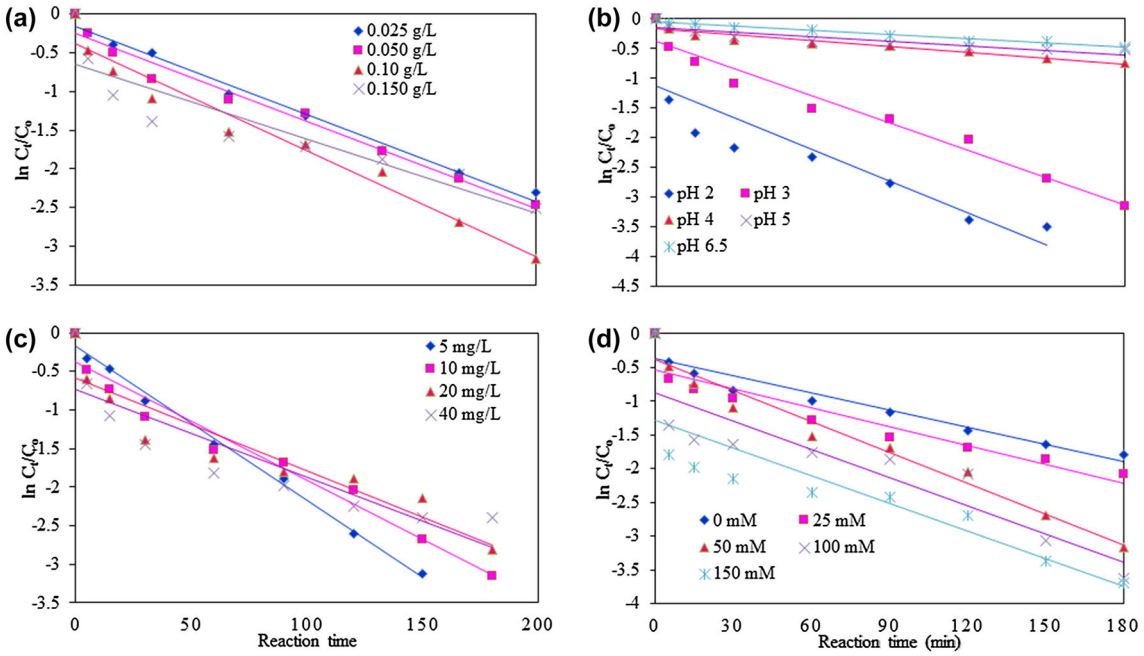

Fig. 4 Kinetic study of CR degradation by NMPs with different parameters: NMPs dose (**a**), pH values (**b**), initial concentration of CR (**c**) and amount of H_2O_2 (**d**)

which can reduce degradation efficiency of pollutants [29]. Many researchers have reported that most of advanced Fenton's processes depend on pH and acidic conditions, which are favorable to the reaction [30, 31]. The effects of pH values (pH 2.0, 3.0, 4.0, 5.0 and 6.5) on the removal of CR were studied. The experimental conditions were: dose of NMPs—0.10 g/L, CR initial concentration—10 mg/L, temperature—25 °C and concentration of H_2O_2—50 mM (Fig. 3b). The degradation efficiency of CR was achieved approximately 97.9% in 180 min of reaction time at pH of 2.0. The degradation efficiencies of CR were decreased from 97.9 to 37.8% with increasing pH from 2 to 6.5 in a

Table 2 Kinetic results for CR degradation by NMPs under Fenton-like process

NMPs dose (g/L)	C_0 (CR) (mg/L)	Initial pH	H_2O_2 conc. (mM)	Pseudo-first-order		Pseudo-second-order	
				k_1 (min^{-1})	R^2	k_2 (L/mg min)	R^2
0.025	10	3.0	50	0.0126	0.9880	0.0048	0.9611
0.05	10	3.0	50	0.0126	0.9754	0.0053	0.9266
0.10	10	3.0	50	0.0153	0.9637	0.0104	0.8524
0.15	10	3.0	50	0.0107	0.8342	0.005	0.9218
0.10	5	3.0	50	0.0199	0.9930	0.0414	0.7818
0.10	20	3.0	50	0.0120	0.8711	0.0033	0.8481
0.10	40	3.0	50	0.0113	0.8036	0.0014	0.9656
0.10	10	2.0	50	0.0179	0.7824	0.0229	0.9558
0.10	10	4.0	50	0.0034	0.9055	0.0005	0.9514
0.10	10	5.0	50	0.0025	0.8163	0.0003	0.8631
0.10	10	6.5	50	0.0024	0.9765	0.0003	0.9830
0.10	10	3.0	0	0.0085	0.9217	0.0025	0.9842
0.10	10	3.0	25	0.0093	0.8790	0.0034	0.9864
0.10	10	3.0	100	0.0139	0.8036	0.0151	0.7352
0.10	10	3.0	150	0.0136	0.7308	0.0174	0.8588

reaction time of 180 min; this can be due to the decrease in activity of the NMPs [32]. Figure 4b shows the plot of ln C_t/C_o versus t for the removal of CR with the various values of pH. The values of k_1 and k_2 were reduced around 86.6 and 98.7%, respectively, when the value of pH was increased from 2.0 to 6.5 (Table 2). Remarkably, rapid degradation of CR was detected at pH 2.0 of CR solution. The results also stated that reaction rate was decreased with increasing pH values, and the oxides of metals were available on the surfaces of NMPs, which were rapidly dissolved in acidic solution and the active sites are free and enhancing corrosion of metals including Fe [8]. At pH 2 of solution, more hydroxyl radicals were generated, which caused the very fast degradation of CR [27]. At pH 4, 5 and 6.8 limited the removal of CR was achieved due to the low concentration of H^+ occurs in the solution, consequentially low generation of hydroxyl radicals. Furthermore, metals hydroxides are generated with the increase in the pH from 4 to 6.8 during the reaction. The accumulation of metal hydroxide precipitates on the surface of NMPs will hinder the generation of reactive oxygen species and decrease the MB removal [28].

Effect of initial concentrations of CR on the degradation of CR

Figure 3c shows the effect of initial CR concentrations (5, 10, 20 and 40 mg/L) on the degradation rate under the following experimental conditions: dose of NMPs—0.10 g/L, initial pH—3.0, temperature—25 °C and concentration of H_2O_2—50 mM. Degradation efficiency of CR was decreased from 97.9 to 91.0% with an increasing initial concentration from 5 to 40 mg/L. The active sites of NMPs were occupied by an increasing CR concentration. Figure 4c demonstrates the plot of ln C_t/C_o versus t for degradation of CR with the different concentrations of CR. The values of k_1 and k_2 were decreased around 43.2 and 96.6%, respectively, with increasing initial CR concentrations from 5 to 40 mg/L. Reduction in the rate of degradation of CR with high concentration of dye may be due to the adsorption of dye molecule on the surface of NMPs, and it could occupy the active sites of NMPs [27]. The values of k_1, k_2 and R^2 for the degradation rate of CR with various concentrations of CR are given in Table 2. The slow degradation of CR after 60 min of reaction time may be clarified by the difficulty in changing the N atoms of the CR into oxidized nitrogen compounds and the slow reaction of short chain aliphatics with hydroxyl radicals; furthermore, the higher number of azo-groups in dye molecule decreases the degradation process [33].

Effect of the H_2O_2 addition on CR degradation

As shown in Fig. 3d, the effect of H_2O_2 concentrations (0, 25, 50, 100 and 150 mM) on the degradation rate was studied under the following experimental condition: dose of NMPs—0.10 g/L, pH value—3.0, temperature—25 °C and initial concentration of CR—10 mg/L. The CR degradation rate was found to be low with NMPs and without addition of H_2O_2; this is because of insufficient or

Table 3 Comparative study for the degradation of CR by different nanomaterials

Nano materials applied	Method of degradation	Reaction time (mins)	Removal (%)	References
ZnO-Pd	Photocatalytic	180	100	[35]
CuO, nano-rod	Photocatalytic	210	67	[36]
Carissa edulis extract capped ZnO nanoparticles	Photocatalytic	130	97	[37]
ZnO	Photocatalytic	80	95.02	[38]
TiO_2	Photocatalytic	30	93.9	[39]
Fe_3+/$(NH_4)_2S_2O_8$/UV	Photo-Fenton process	50	100	[40]
NMPs	Advanced Fenton's process	180	99.8	Present study

no creation of hydroxyl radicals during the reaction. The hydroxyl radical is one of the most strongest oxidizing agents, which attacks organic compounds present at the surface of the NMPs [27]. The CR removal efficiency was increased from 83.2 to 95.8% by increasing the concentration of H_2O_2 from 0 to 50 mM; this is due to the generation of huge amount of hydroxyl radicals [27]. However, with a further increase in the concentration of H_2O_2, degradation efficiency was decreased slightly; this can be attributed to recombination of hydroxyl radicals and scavenging effect of H_2O_2, causing decrease in the oxidation of NMPs by H_2O_2 [14]. Furthermore, hydroperoxyl radicals were generated from the excess hydroxyl radicals, which were not participated in the oxidative degradation of the CR due to very less reactivity of hydroperoxyl radicals. The degradation of the CR was found by mainly reaction with hydroxyl radicals [1]. Figure 4d displays the plot of ln C_t/C_o versus t for the degradation of CR with various concentrations of H_2O_2. The value of k_1 was increased around 80% with an increasing concentration of H_2O_2 up to 50 mM. However, with further increase in the concentration of H_2O_2, a value of k_1 was slightly reduced. However, the value of k_2 was increased with increasing concentration of H_2O_2 from 0 to 150 mM. The removal efficiency of CR was enhanced suggestively in the combination of NMPs and hydrogen peroxide in acidic pH of solution as compared to the NMPs alone. Table 2 shows the values of k_1, k_2 and R^2 for the degradation rate of CR with various concentrations of H_2O_2.

Probable mechanism for the removal of CR by NMPs

The oxidation of CR by hydroxyl radicals was mainly responsible for the degradation of CR in an aqueous solution. Hydroxyl radicals are generated when NMPs can react with the aqueous H_2O_2 [28]. The highest rate of CR degradation may be due to the high corrosion of NMPs at acid pH of solution and availability of numerous active sites for reaction. An oxidation of CR by H_2O_2 in the acidic pH of solution was mainly due to the generation of hydroxyl radicals in the reaction [34]. The removal mechanism of CR using NMPs can be expressed as follows [14]:

$$\text{NMPs} + H_2O_2 + H^+ \rightarrow M^{n+} + OH^{\cdot} + OH^- \quad (3)$$

$$M^{n+} + H_2O_2 \rightarrow M^{(n+1)+} \rightarrow OH^{\cdot} + OH^- \quad (4)$$

$$OH^{\cdot} + \text{CR} \rightarrow \text{Intermediate} + CO_2 + H_2O \quad (5)$$

$$M_xO_y + nH^+ \rightarrow nM^{n+} + nH_2O \quad (6)$$

where "M" represents metal, "n" is number of valences or moles, and "O" represents oxides.

The studies on degradation of Congo red have been represented in Table 3. When NMPs compared with all other catalyst showed almost highest % degradation than other materials such as Carissa edulis extract capped ZnO, ZnO and TiO_2 nanoparticles.

Conclusion

The degradation of CR by NMPs in the presence of H_2O_2 was found to be highly effective. The CR degradation efficiencies were increased from 90.1 to 95.8% with increasing the dosages of NMPs from 0.025 to 0.10 g/L and further increase in dosages, efficiency was not increased. However, degradation efficiency was decreased from 97.9 to 37.8% with increasing the value of pH from 2.0 to 6.5. The degradation efficiency of CR was reduced with an increasing concentration of CR. However, degradation efficiency was increased with an increasing concentration of H_2O_2 up to certain limit. The degradation efficiency of CR by NMPs was most suitable under acidic pH of solution. The degradation of CR by NMPs under Fenton-like process followed the pseudo-second-order kinetics as compared to the pseudo-second-order kinetics. A very fast degradation rate was attained at pH 2.0 of CR solution. The present study confirmed that the CR can be removed successfully by even very small amount of NMPs under the Fenton-like process.

Acknowledgements This study has been conducted by the research grant of Kwangwoon University in 2017. This work was also supported by the UGC-BSR Research startup grant (No. F. 30-382/2017, BSR), Government of India.

References

1. Kondru AK, Kumar P, Chand S (2009) Catalytic wet peroxide oxidation of azo dye (Congo red) using modified Y zeolite as catalyst. J Hazard Mater 166:342–347
2. Sha Y, Mathew I, Cui Q, Clay M, Gao F, Zhang XJ, Gu Z (2016) Rapid degradation of azo dye methyl orange using hollow cobalt nanoparticles. Chemosphere 144:1530–1535
3. Li P, Song Y, Wang S, Tao Z, Yu S, Liu Y (2015) Enhanced decolorization of methyl orange using zero-valent copper nanoparticles under assistance of hydrodynamic cavitation. Ultrason Sonochem 22:132–138
4. Goudarzi M, Bazarganipour M, Salavati-Niasari M (2014) Synthesis, characteriza-tion and degradation of organic dye over Co_3O_4 nanoparticles prepared from new binuclear complex precursors. RSC Adv 4(87):46517–46520
5. Manivel A, Lee G-J, Chen C-Y, Chen J-H, Ma S-H, Horng T-L, Wu JJ (2015) Synthesis of MoO_3 nanoparticles for azo dye degradation by catalytic ozonation. Mater Res Bull 62:184–191
6. Nidheesh P, Gandhimathi R, Ramesh S (2013) Degradation of dyes from aqueous solution by Fenton processes: a review. EnvironSci Pollut Res 20(4):2099–2132
7. Singla P, Sharma M, Pandey OP, Singh K (2014) Photocatalytic degradation of azo dyes using Zn-dopedand undoped TiO_2 nanoparticles. Appl Phys A 116(1):371–378
8. Fang ZQ, Qiu XQ, Chen JH, Qiu XH (2010) Degradation of metronidazole by nanoscale zero-valent metal prepared from steel pickling waste liquor. Appl Catal B Environ 100:221–228
9. Shih Y-H, Tso C-P, Tung L-Y (2008) Rapid degradation of methyl orange with nanoscale zerovalent iron particles. Nanotechnology 7:16–17
10. Bokare AD, Chikate RC, Rode CV, Paknikar KM (2008) Iron-nickel bimetallic nanoparticles for reductive degradation of azo dye Orange G in aqueous solution. Appl Catal B Environ 79(3):270–278
11. Rani S, Sumanjit K, Mahajan RK (2016) Synthesis of mesoporous material SBA-3 for adsorption of dye congo red. Desalination Water Treat 57(8):3720–3731
12. Kaur S, Rani S, Kumar V, Mahajan RK, Asif M, Tyagi I, Gupta VK (2015) Synthesis, characterization and adsorptive application of ferrocene based mesoporous material for hazardous dye Congo red. J Ind Eng Chem 26:234–242
13. Sumanjit Seema, Mahajan RK, Gupta VK (2015) Modification of surface behaviour of *Eichhornia crassipes* using surface active agent: an adsorption study. J Ind Eng Chem 21:189–197
14. Singh J, Yang JK, Chang YY (2016) Rapid degradation of phenol by ultrasound-dispersed nano-metallic particles (NMPs) in the presence of hydrogen peroxide: a possible mechanism for phenol degradation in water. J Environ Manage 175:60–66
15. Singh J, Lee BK (2015) Pollution control and metal resource recovery for low grade automobile shredder residue: a mechanism, bioavailability and risk assessment. Waste Manage 38:271–283
16. Singh J, Yang JK, Chang YY (2016) Quantitative analysis and reduction of the eco-toxicity risk of heavy metals for the fine fraction of automobile shredder residue (ASR) using H_2O_2. Waste Manage 48:374–382
17. Singh J, Lee BK (2015) Reduction of environmental availability and ecological risk of heavy metals in automobile shredder residues. Ecol Eng 81:76–81
18. Rasheed QJ, Pandian K, Muthukumar K (2011) Treatment of petroleum refinery wastewater by ultrasound-dispersed nanoscale zero-valent iron particles. Ultrason Sonochem 18:1138–1142
19. Singh J, Lee BK (2015) Hydrometallurgical recovery of heavy metals from low-grade automobile shredder residue (ASR): an application of an advanced Fenton process (AFP). J Environ Manage 161:1–10
20. Fang ZQ, Qiu XH, Chen JH, Qiu XQ (2011) Debromination of polybrominated diphenyl ethers by Ni/Fe bimetallic nanoparticles: influencing factors, kinetics, and mechanism. J Hazard Mater 185:958–969
21. Zha SX, Cheng Y, Gao Y, Chen ZL, Megharaj M, Naidu R (2014) Nanoscale zerovalent iron as a catalyst for heterogeneous Fenton oxidation of amoxicillin. Chem Eng J 255:141–148
22. Yuan SJ, Dai XH (2014) Facile synthesis of sewage sludge-derived mesoporous material as an efficient and stable heterogeneous catalyst for photo-Fenton reaction. Appl Catal B Environ 154–155:252–258
23. Singh J, Lee BK (2016) Recovery of precious metals from low-grade automobile shredder residue: a novel approach for the recovery of nano zero-valent copper particles. Waste Manage 48:353–365
24. Zhou JY, Yu XJ, Ding C, Wang ZP, Zhou QQ, Pao H, Cai WM (2011) Optimization of phenol degradation by Candida tropicalis Z-04 using Plackette Burman design and response surface methodology. J Environ Sci 23:22–30
25. Fan J, Guo Y, Wang J, Fan M (2009) Rapid decolorization of azo dye methyl orange in aqueous solution by nanoscale zerovalent iron particles. J Hazard Mater 166:904–910
26. Chen H-L, Chiang T-H, Wu M-C (2012) Evolution of morphology of nano-scale CuO grown on copper metal sheets in 5 wt% NaCl solution of spray fog environment. J Surf Eng Mater Adv Technol 2:278–283
27. Xu L, Wang J (2011) A heterogeneous Fenton like system with nanoparticulate ZVI for removal of 4 chloro 3 methyl phenol. J Hazard Mater 186:256–264
28. Cheng Z, Fu F, Pang Y, Tang B, Lu J (2015) Removal of phenol by acid-washed zero-valent aluminium in the presence of H_2O_2. Chem Eng J 260:284–290
29. Tian H, Li JJ, Mu Z, Li LD, Hao ZP (2009) Effect of pH on DDT degradation in aqueous solution using bimetallic Ni/Fe nanoparticles. Sep Purif Technol 66(1):84–89
30. Bokare AD, Choi W (2009) Zero-valent aluminum for oxidative degradation of aqueous organic pollutants. Environ Sci Technol 43:7130–7135
31. Liu WP, Zhang HH, Cao BP, Lin K, Gan J (2011) Oxidative removal of bisphenol A using zero valent aluminum-acid system. Water Res 45:1872–1878
32. Babuponnusami A, Muthukumar K (2012) Removal of phenol by heterogeneous photo electro Fenton-like process using nano-zero valent iron. Sep Purif Technol 98:130–135
33. Ljubas D, Smoljani G, Jureti H (2015) Degradation of methyl orange and congo red dyes by using TiO_2 nanoparticles activated by the solar and the solar-like radiation. J Environ Manage 161:83–91
34. Yang S, Wang P, Yang X, Shan L, Zhang W, Shao X, Niu R (2010) Degradation efficiencies of azo dye acid orange 7 by the interaction of heat, UV and anions with common oxidants: persulfate, peroxymonosulfate and hydrogen peroxide. J Hazard Mater 179:552–558
35. Rokesh K, Pandikumar A, Jeganathan K, Jothivenkatachalam K (2016) Zinc oxide nanostructures and their morphology depended optical, crystalline and photocatalytic properties. Mater Focus 5:385–392
36. Sadollahkhani A, Ibupoto ZH, Elhag S, Nur O, Willander M (2014) Photocatalytic properties of different morphologies of

CuO for the degradation of Congo red organic dye. Ceram Int 40:11311–11317
37. Fowsiya J, Madhumitha G, Al-Dhabi NA, Arasu MV (2016) Photocatalytic degradation of Congo red using Carissa edulis extract capped zinc oxide nanoparticles. J Photochem Photobiol B 162:395–401
38. Laouedj EN, Ahmed B (2011) ZnO assisted photocatalytic degradation of Congo red and Benzopurpurine 4B in aqueous solution. Chem Eng Process Technol 2:1–9
39. Erdemoglu S, Aksu SK, Sayilkan F, Izgi B, Asiltürk M, Sayilkan H, Frimmel F, Güçer S (2008) Photocatalytic degradation of Congo Red by hydrothermally synthesized nanocrystalline TiO_2 and identification of degradation products by LC-MS. J Hazard Mater 155:469–476
40. Gomathi Devi L, Girish Kumar S, Mohan Reddy K (2009) Photo fenton like process Fe_3 +/$(NH_4)_2S_2O_8$/UV for the degradation of Di azo dye congo red using low iron concentration. Cent Eur J Chem 7(3):468–477